J. Appl. Comput. Mech., xx(x) (2026) 1-15
DOI: 10.22055/jacm.2026.49109.5741

ISSN: 2383-4536
jacm.scu.ac.ir

Shahid Chamran University of Ahvaz

Journal of
Applied and Computational Mechanics

Research Paper

Numerical Investigation of Two-Phase Flow Transition and Heat Transfer in a V-Shaped Cavity with Stratified Fluids

Md. Mahafujur Rahaman[1,2], Sidhartha Bhowmick[2], Goutam Saha[3], Suvash C. Saha[4]

[1] Department of Computer Science and Engineering, Z. H. Sikder University of Science and Technology, Shariatpur, 8024, Bangladesh, Email: mahfuz0809@gmail.com

[2] Department of Mathematics, Jagannath University, Dhaka, 1100, Bangladesh, Email: sidharthabhowmick@yahoo.com

[3] Department of Mathematics, International University of Business Agriculture and Technology, Dhaka-1230, Bangladesh, Email: gsahamath@du.ac.bd

[4] School of Mechanical and Mechatronic Engineering, University of Technology Sydney, Ultimo, North South Wales, 2007, Australia, Email: suvash.saha@uts.edu.au

Received January 30 2026; Revised August 11 2026; Accepted for publication August 12 2026.
✉ Corresponding author: M.M. Rahaman (mahfuz0809@gmail.com)

Abstract. Two-phase air-water flow is very important in many industrial systems, including chemical reactors, nuclear power plants, refrigeration systems and petrochemical technologies. Motivated by their relevance, the present work examines natural convection (NC), heat transfer (HT), and entropy generation (E_{gen}) inside a V-shaped cavity containing two stratified fluids, namely air and water. The numerical simulations are performed applying the volume of fluid (VOF) method, which effectively captures interfacial dynamics between the phases. The physical configuration studied is one where water is filled in the lower part of the cavity, while air is filled in the upper part of the cavity and the heating is applied at the fluid interface. Thermal stratification is applied on the inclined walls, from the interface to the top in the air phase and from the interface to the bottom in the water phase. User-defined functions (UDFs) are used in FLUENT to apply thermal boundary conditions and the governing equations are discretized by using finite volume method (FVM). The VOF model numerically simulates the transport equations for each phase individually and couples them together through the interaction forces on the interfaces. The simulations are carried out by using Prandtl number (Pr) of 0.71 for air and 7.01 for water and Rayleigh number (Ra) ranging from 10^0 to 10^8. Streamline and isotherm distributions, temperature time series (TTS), bifurcation analyses, average Nusselt number (Nu_{avg}) time series, E_{gen}, and average Bejan number (Be_{avg}) distributions are used to analyze the flow and thermal characteristics. The results show a series of transitions from steady to chaotic flow as Ra is increased. A pitchfork bifurcation is observed in both phases between Ra = 9×10^5 and 10^6. Subsequently, a Hopf bifurcation is identified in the air phase between Ra = 5×10^6 and 10^7. In the air phase, a transition from periodic to chaotic flow occurs at Ra = 5×10^7, while the flow in the water phase remains in a weakly rotational state. Moreover, at higher Ra, E_{gen} due to fluid friction (FF) becomes dominant in the air phase. The findings also show that both the HT rate and E_{gen} in the air phase is significantly greater than that in the water phase.

Keywords: Stratified fluid; Two-phase flow; Natural convection; Entropy generation; VOF method.

1. Introduction

The study of air–water flow dynamics in natural systems under ambient environmental conditions constitutes a fundamental aspect of environmental fluid mechanics (EFM). Since its emergence several decades ago, EFM has focused on understanding the transport and flow behavior of air and water within a relatively narrow range of natural temperatures and pressures. These studies cover a wide range of environmental systems, including lakes, rivers, estuaries, groundwater reservoirs and atmospheric flows. EFM has attracted considerable interest from engineers, scientists, and policymakers because it plays a key role in understanding as well as managing environmental processes. Related fields, such as meteorology, geophysical fluid dynamics and oceanography, deal with large-scale atmospheric and oceanic flows. EFM deals mainly with phenomena on the local to regional scale that have directs implications for human activities and engineering systems. The HT induced by NC in stratified media is among these phenomena of special interest because of its regular occurrence in natural environment and engineering applications. Such flows are generally unsteady, highly nonlinear, and thermally coupled, thereby requiring rigorous numerical and theoretical analyses to clarify their underlying dynamics.

Over the past several decades, numerous studies have investigated unsteady NC and HT characteristics in single-phase fluids using different computational approaches and cavity geometries. The first study of this kind was done by Patterson and Imberger [1] who examined unsteady NC in a rectangular cavity and presented detailed numerical solutions for the time evolution of the flow field. Their study also developed validation criteria for NC systems based on scale analysis. Subsequently, Lin et al. [2] investigated transient NC boundary-layer flow adjacent to a vertically heated plate embedded in a thermally stratified fluid with a

Published online: September 03 2026

Pr less than unity. In their work they proposed scaling relations for low-Pr fluids and clarified the role of thermal diffusivity in the transient regime. Lie et al. [3] later explored unsteady NC within a triangular cavity occupied with water and demonstrated the occurrence of pitchfork bifurcations. More recently, HT characteristics in square and rectangular cavities with different working fluids were numerically explored by Shaon and Rahaman [4], Hossain et al. [5] and Shaon et al. [6]. Bhowmick et al. [7] showed that the initial density stratification has a substantial influence on the beginning of convection and evolution of flow in V-shaped cavities. Recently, Rahaman et al. [8] examined unsteady NC in trapezoidal cavity containing stratified fluid. Their study identified critical Ra values associated with various bifurcation transitions and quantified the corresponding variations in HT rates under different Ra.

In contrast to single-phase systems, two-phase fluid flows are manifested extensively in engineering applications, for example nuclear reactors, petrochemical equipment, refrigeration systems, and heating, ventilation, as well as air-conditioning (HVAC) technologies. In these systems, single-phase models are often inadequate for accurately describing the complex interactions between phases, interfacial transport phenomena, and thermohydrodynamic behavior. Consequently, extensive experimental and computational investigations have been keen to comprehending two-phase flow dynamics in various geometries. Hanafizadeh et al. [9] categorized the flow regimes of air-water flow in perpendicular mini pipes and determined the borderlines between bubbly, slug, churn and annular flow patterns. Zhang et al. [10] applied 3D reconstruction technology and VOF simulation to investigate the horizontal mini-tubes and achieved good prediction of pressure drop and interfacial characteristics. Talley et al. [11] made use of high-speed imaging to observe flow regimes in horizontal round pipes. The study of Dassler and Janoske [12] demonstrated the effects of bend and inertial effects on the pressure losses in the rectangular 180° return bends and Zahedi and Rad [13] studied numerically and experimentally the flow development and the pressure drop in the 90° elbows. Kükrer and Eskin [14] also found the void fraction distribution in U-bend geometries and showed how the phase redistribution due to curvature has an important effect on the flow behaviour. All of these investigations demonstrated the critical role geometry and scale play in the characterization of two-phase flow dynamics. The pressure drop phenomena of gas-liquid flow in flattened tube was also investigated by experimental and computational studies by Yaqop [15] and the influence of non-circular cross-sectional geometry of the flattened tube on two-phase flow behavior has been emphasized. Yin et al. [16] further showed in their experimental and computational study of the vertical upward gas-liquid flow in a large annulus that the confinement and the geometrical scale also play an important role in affecting the phase distribution and the hydrodynamic characteristics. More recently, Lv et al. [17] experimentally and computationally investigated convective HT in gas-liquid flows, also discussed the underlying mechanisms regarding different flow regimes. They found that the interaction among gas bubbles, liquid motion, turbulence and thermal gradients can have a significant impact on their results. Furthermore, Huang et al. [18] investigated the performance of HT and pressure drop of different gas-liquid flow patterns in microchannels by experiment. All these studies demonstrated the role of geometry and scale in the control of the two-phase flow behavior.

Several classic studies have also theoretically justified the characterization of gas-liquid flow regimes. Under the boiling conditions, the complicated relationship between two-phase dynamics and HT was investigated by Li et al. [19] about critical heat flux in microchannels with two-phase oscillation caused by microbubbles. Tiwari and Moharana [20] numerically investigated the strong coupling between phase distribution and thermal transport in the two-phase flow of thrugh a microtube. Nishio and Kurose [21] numerically studied the gas-liquid two-phase flow in a horizontal manifold and saw that the complex geometry of the manifold can significantly influence the phase distribution and flow characteristics. The local geometric restrictions play a vital role in the flow structure and pressure behavior in the gas-liquid two-phase flow in a flat pipe with the orifice plate, which was computationally investigated by Zhang et al [22]. However, Sheng et al. [23] highlighted the fundamental hydrodynamic characteristics of micro gas-liquid flows and demonstrated the role of flow topology, film behavior and confinement effects in the transport behavior of multiphase systems. Experimental techniques are expensive and have limited details, numerical simulation is a cost-efficient and very detailed framework to study two-phase flow phenomena. CFD and electrical resistance tomography techniques were utilized to study two-phase flow in perpendicular and horizontal tubes by Parvareh et al. [24] and it was shown that the orientation has important effects on the flow behavior due to the influences of gravity and buoyancy. Deendarlianto et al. [25] have numerically examined the gas-liquid plug flow in flat pipes and provided explanation on the evolution and dynamics of the plug structures for various flow conditions. López et al. [26] investigated liquid-gas flow in horizontal pipes and reported extensive work on the interfacial dynamics and flow development. Georgoulas et al. [27] presented an enhanced VOF approach with HT and phase-change mechanisms to investigate the bubble departure in saturated pool boiling. The study revealed the complex interplay of HT and interface evolution of the bubbles during bubble growth and departure. Taking into account the compressibility effects, Shi et al. [28] proposed a numerical model for gas-liquid flow with phase-change HT using OpenFOAM. The study emphasized the importance of the proper coupling at the interface, the change of the phase and the transfer of heat to predict multiphase systems. Xiaoqi et al. [29] has also numerically studied the interfacial waves of the liquid film under the gas-liquid two-phase flow with the help of OpenFOAM. Their results highlighted the relevance of the development of interfacial waves on the local flow structure and transport phenomena.

However, these significant advances have been mainly focused on the first law of thermodynamics, considering the energy conservation and the HT performance, frequently neglecting the thermodynamic irreversibilities related to E_{gen}, for most of the two-phase flow investigations. Though, Bejan [30] provided a thermodynamic approach based on the second law for single-phase systems that enables the calculation of irreversibility in thermal systems. Later this concept has been prolonged to the formulation of the entropy generation minimization (EGM) framework [31], which quantifies the energy degradation and provides a basis for the thermodynamic efficiency optimization. In recent years, EGM has been developed as a powerful analytical tool to measure and optimize the performance of thermofluid systems. The EGM approach has been successfully used in a number of studies [32, 33] for the analyses of system performance and optimization of thermal processes. Entropy generation in NC was investigated in variously heated rectangular cavities by Magherbi et al. [34] and Ilis et al. [35], offering relevant reference data for entropy-based analysis. Later on, Varol et al. [36], Basak et al. [37] and Siavashi et al. [38] studied the combined effects of HT and FF irreversibility in complex systems like porous media systems. These studies have all helped to solidify EGM as a fundamental framework to understand and optimize advanced thermal systems.

While significant advances have been made in the understanding of single-phase NC, phase change phenomena and porous-media convection, the computational analyses of two-phase NC flows are still relatively limited. Many engineering and practical applications such as chemical reactors, petroleum transportation system, nuclear reactors, compact heat exchangers, microfluidic devices, thermal management systems and energy conversion technologies are faced with gas-liquid two-phase flows. The coupled interactions among buoyancy forces, interfacial dynamics, thermal gradients and phase distribution can result in highly complex flow structures and HT mechanisms in such type of systems, which are fundamentally different from what are seen in single phase flows. In the present study, a V-shaped cavity is used as a representative geometry of cavity having inclined surfaces at a given angle and specific boundaries. The V-shaped cavity is not only an idealized geometry, but also natural valley-like topographies that are often found in mountainous and hilly areas. These valleys are frequently filled with air and water, and represent a system of two-phases with environmental conditions. The role of HT caused by NC in controlling the circulation and thermal stratification in these regions of valleys is important. They have direct impacts on environmental processes like fog formation and dissipation, frost occurrence, moisture transport and local microclimatic conditions. Thus, the air-water interaction in a V-shaped cavity can provide basic understanding of environmental fluid dynamics, especially under conditions of thermal instabilities, that can control the steady to unsteady flow transition. Besides the environmental applications, V-shaped cavities are also found in engineering systems such as solar thermal collector with V-grooved absorber, passive cooling channel, roof valley, drainage system and V-groove heat exchanger, where buoyancy-induced flow is important for thermal performance. In the present study, the evolution of flow instability, HT characteristics and interface dynamics for such two-phase NC is studied over a broad range of Ra in order to advance the fundamental understanding of such NC.

Despite the practical relevance of these configurations, the coupled behaviour of two-phase NC, HT, and E_{gen} in V-shaped cavities has not been investigated in detail. There has not been any previous work, to the best of the authors' knowledge, that has systematically investigated unsteady NC and E_{gen} in a V-shaped cavity that involves a stratified air-water two-phase system. In the present study, this research gap is filled with a detailed numerical study of the unsteady NC, HT and E_{gen} in a V-shaped cavity filled with stratified air and water, by using the VOF technique. Special attention is paid to the effect of thermal boundary conditions on the HT characteristics, quantification of E_{gen} resulting from thermal and FF irreversibilities, and the evaluation of the Be_{avg} to determine relative contributions of HT and FF irreversibilities to the overall thermodynamic phenomena of the system. The results offer new insight into the coupled thermal, hydrodynamic and thermodynamic properties of two-phase NC in complex geometries, and helps to develop a broader understanding of the flow mechanisms underpinning HT enhancement and thermodynamic optimization in gas-liquid thermal systems.

2. Physical and Computational Model

In the present study unsteady NC and HT characteristics in a two-phase fluid system inside a V-shaped cavity are investigated. The computational domain comprises a cavity of height H and top length $2L$. The geometric relation $L = H$ is maintained, resulting in an aspect ratio $AR = H/L$. A schematic representation of the physical configuration and allied boundary conditions is demonstrated in Fig. 1. The cavity is thermally configured such that the top horizontal wall is sustained at a constant cooled temperature, T_c, while a constant heated temperature, T_h, is imposed along the air-water interface. The inclined sidewalls are subjected to thermal stratification boundary conditions, where the temperature varies along the y-axis. In the air phase, the temperature varies linearly from the interface toward the upper section of the cavity, while in the water phase, thermal stratification is imposed from the interface toward the lower section. The cavity is vertically divided into two equal halves, where the upper half is occupied by stably stratified air and the lower half by stably stratified water. UDFs are adopted in ANSYS FLUENT to correctly implement the thermal boundary conditions at the fluid interface and inclined walls. Since sharp geometric corners may introduce numerical singularities and adversely affect solution convergence, the sharp tips positioned at the upper and lower ends of the inclined walls are truncated. Each truncated section corresponds to approximately 4% of the total characteristic length L. The resulting vertical tips are treated as adiabatic, whereas the horizontal bottom tip is maintained at the cooled temperature T_c. All cavity walls are considered to be rigid and satisfy the no-slip condition.

2.1. Governing equations

In this study, thermal radiation and evaporation effects are disregarded. The flow is presumed to be 2D, transient, and incompressible. The working fluids are considered Newtonian with fixed thermophysical properties, excluding for the density variation, which is incorporated through the Boussinesq approximation. Accordingly, the dimensionless governing equations adopted in the present analysis are formulated under the Boussinesq assumption and are expressed as follows [39, 40]:

$$\frac{\partial u}{\partial x}+\frac{\partial v}{\partial y}=0, \tag{1}$$

$$\frac{\partial u}{\partial \tau}+u\frac{\partial u}{\partial x}+v\frac{\partial u}{\partial y}=-\frac{\partial p}{\partial x}+\frac{\mathrm{Pr}}{\sqrt{\mathrm{Ra}}}\left(\frac{\partial^2 u}{\partial x^2}+\frac{\partial^2 u}{\partial y^2}\right), \tag{2}$$

$$\frac{\partial v}{\partial \tau}+u\frac{\partial v}{\partial x}+v\frac{\partial v}{\partial y}=-\frac{\partial p}{\partial y}+\frac{\mathrm{Pr}}{\sqrt{\mathrm{Ra}}}\left(\frac{\partial^2 v}{\partial x^2}+\frac{\partial^2 v}{\partial y^2}\right)+\mathrm{Pr}\,\theta+f_s, \tag{3}$$

$$\frac{\partial \theta}{\partial \tau}+u\frac{\partial \theta}{\partial x}+v\frac{\partial \theta}{\partial y}=\frac{1}{\sqrt{\mathrm{Ra}}}\left(\frac{\partial^2 \theta}{\partial x^2}+\frac{\partial^2 \theta}{\partial y^2}\right). \tag{4}$$

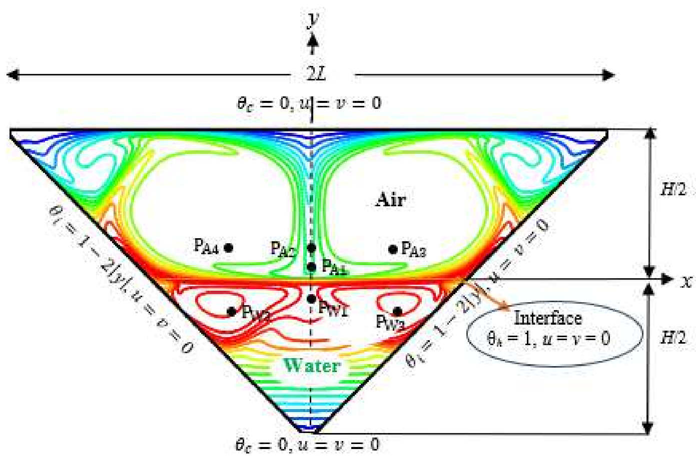

Fig. 1. Schematic of geometric configuration and dimensionless boundary conditions.

The final term in Eq. (3) represents the normalized surface tension force. The successive are the dimensionless variables:

$$x=\frac{X}{Y},y=\frac{Y}{H},u=\frac{UH}{\kappa\sqrt{\mathrm{Ra}}},v=\frac{VH}{\kappa\sqrt{\mathrm{Ra}}},p=\frac{PH^2}{\rho\kappa^2\mathrm{Ra}},\theta=\frac{T-T_\infty}{T_h-T_c},\tau=\frac{t\kappa\sqrt{\mathrm{Ra}}}{H^2},f_s=\frac{F_sH^3}{\rho\kappa^2\mathrm{Ra}}. \tag{5}$$

In the above equations u, v, x, y, p, τ, f_s, and θ are the normalized form of U, V, X, Y, P, t, F_s, and T. Three results monitoring parameters in the cavity: AR, Pr, and Ra, are defined as:

$$\mathrm{AR}=\frac{H}{L},\mathrm{Pr}=\frac{\nu}{\kappa},\text{and }\mathrm{Ra}=\frac{g\beta(T_h-T_c)H^3}{\nu\kappa}. \tag{6}$$

The normalized boundary conditions for temperature and velocity are:

$$\begin{cases}\theta_c=u=v=0,\text{at the bottom and top walls;}\\ \theta_h=1,\ u=v=0,\text{at the interface of the cavity;}\\ \theta_i=1-2|y|,\ u=v=0,\text{at the sloped walls.}\end{cases} \tag{7}$$

2.2. VOF model

In the present study, VOF model is employed in ANSYS FLUENT 17.0 for simulating the two-phase flow behavior inside the cavity. The VOF method is particularly appropriate for capturing and tracking the interface between immiscible fluids and has been widely used in the analysis of multiphase flow systems. In this study, air and water are supposed to be incompressible and immiscible fluids. In the VOF formulation, the phases are assumed to be physically separated without interpenetration through the flow domain.

The volume fraction (VF) of each phase in the computational cells is introduced and the governing equations are solved in the VOF framework. A particular phase k is characterized by its local VF, α_k, in the computational domain. When α_k = 1.0, the corresponding cell is completely occupied by stratified water, whereas α_k = 0.0 shows that the cell is entirely filled with stratified air, as illustrated in Fig. 2. For intermediate values of α_k ($0.0 < \alpha_k < 1.0$), the cell comprehends in the interface separating the air and water phases. The summation of the VFs of all phases within each control volume (CV) satisfies the following relation [40]:

$$\sum_{k=1}^{n}\alpha_k=1.0. \tag{8}$$

The evolution of the phase interface is determined by solving the continuity equation for the VF of each phase. For the k^{th} phase, the governing VF transport equation is formulated as [39, 40]:

$$\frac{\partial\alpha_k}{\partial\tau}+\alpha_k\left(\frac{\partial u}{\partial x}+\frac{\partial v}{\partial y}\right)=0. \tag{9}$$

Using the local VF values, α_k, the thermophysical properties and flow variables are allocated to each CV inside the cavity. In a two-phase system, where the individual phases are denoted by subscripts 1 and 2, and the VF of the second phase is being tracked, the effective properties within a CV are determined depending on the weighted average of the corresponding phase values. Specifically, the local density, ρ, in each cell is computed as [40]:

$$\rho=\alpha_2\rho_2+(1-\alpha_2)\rho_1. \tag{10}$$

Similarly, all other thermophysical properties, together with dynamic viscosity and thermal conductivity, are resolved using the similar averaging procedures.

In the VOF model, the momentum and energy equations are solved over the whole computational domain, encompassing both fluid phases simultaneously. A single velocity field is computed and shared by the phases, thereby ensuring conservation of momentum and energy across the phase interface. Consequently, the governing equations in Eqs. (2)-(4), inherently depend on the local VF distribution through the actual thermophysical properties.

2.3. Heat transfer and entropy generation

The thermal performance of the cavity is quantified through the evaluation of the Nu_{avg} along the horizontal and inclined walls. The Nu_{avg} along the horizontal and inclined walls, denoted as $[\mathrm{Nu}_{avg}]_h$ and $[\mathrm{Nu}_{avg}]_i$ respectively, are defined as follows [8]:

$$\left[\mathrm{Nu}_{avg}\right]_h=\frac{1}{l}\int_0^1\frac{\partial\theta}{\partial y}dx\text{ and }\left[\mathrm{Nu}_{avg}\right]_i=\frac{1}{l}\int_0^1\frac{\partial\theta}{\partial n}ds. \tag{11}$$

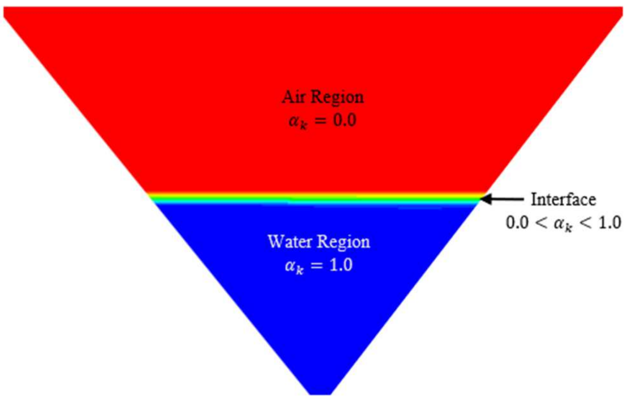

Fig. 2. Visualization of the water-air interface in multi green color.

Table 1. Thermophysical properties of stratified water and air (for details, refer to Yan and Chen [44]).

Property (unit)	Stratified water	Stratified air
C_p (J/kg K)	4182	1012
ρ (kg/m^3)	998.4	1.177
k (W/m K)	0.566	0.0257887
μ (kg/m s)	9.4748×10^{-4}	1.8093×10^{-5}
β (1/K)	3.109×10^{-4}	0.008045
σ (N/m)	0.072 (water/air)	-

According to the principles of local thermodynamic equilibrium and linear transport theory [31], the local E_{gen} due to HT and FF for 2D flow can be expressed explicitly as [39]:

$$E_{ht} = \left(\frac{\partial \theta}{\partial x}\right)^2 + \left(\frac{\partial \theta}{\partial y}\right)^2, \tag{12}$$

$$E_{ff} = \psi\left[2\left\{\left(\frac{\partial u}{\partial x}\right)^2 + \left(\frac{\partial v}{\partial y}\right)^2\right\} + \left(\frac{\partial u}{\partial y} + \frac{\partial v}{\partial x}\right)^2\right]. \tag{13}$$

where E_{ht} and E_{ff} characterize the local E_{gen} due to HT and FF, respectively. In Eq. (13), ψ denotes the irreversibility distribution ratio, which is defined as [39]:

$$\psi = \frac{\mu T_{\infty}}{\kappa}\left(\frac{k}{L\Delta T}\right)^2. \tag{14}$$

In the literature, different values of the irreversibility coefficient ψ have been adopted depending on the level of viscous dissipation considered. For instance, a value of 10^{-4} is commonly used for fluid media [34], whereas Varol et al. [41] employed $\psi = 10^{-3}$, and higher value of $\psi = 10^{-2}$ was later adopted by Varol et al. [42] for evaluating total E_{gen}. In the present study, $\psi = 10^{-2}$ is chosen to maintain consistency with studies involving relatively high irreversibility effects. The total local entropy generation (E_l) within the cavity is computed by adding Eqs. (12) and (13) as [39]:

$$E_l = E_{ht} + E_{ff}. \tag{15}$$

The relative contribution of HT irreversibility to the total E_{gen} is characterized by the Bejan number (Be). The local Bejan number (Be_l) define as (refer to [43]):

$$Be_l = \frac{E_{ht}}{E_{ht} + E_{ff}}. \tag{16}$$

The average Bejan number (Be_{avg}) define as follows, as used in [43]:

$$Be_{avg} = \frac{\int_0^1 \int_0^1 Be_l \, dx\, dy}{\int_0^1 \int_0^1 dx\, dy}. \tag{17}$$

The thermophysical properties of the working fluids are showed in Table 1.

3. Numerical Approach

In this study, numerical simulation of Eqs. (1)-(4) was obtained by using the FVM approach implemented in FLUENT 17.0. The governing equations were solved separately for the water and air phases using the VOF model, while the interfacial dynamics between the phases were captured through appropriate coupling mechanisms to accurately represent phase interactions. The widely adopted SIMPLE algorithm [45] was used to achieve pressure-velocity coupling. The pressure terms were discretized by the PRESTO (Pressure Staggering Option) scheme, and the momentum and energy equations were discretized by a second-order upwind scheme for better numerical accuracy. Advection terms were discretized by the QUICK scheme [46]. Furthermore, time integration terms were discretized employing a second-order implicit difference scheme. To maintain numerical stability and convergence in the iterative solution process, under-relaxation factors were used for the governing equations (for further details, see Ref. [8]). The convergence tolerance for the continuity, momentum, and energy equations was set to 10^{-5}.

4. Model Validation and Grid Dependent Test

4.1. Model validation

Model validation is an integral part of the numerical study. Since the number of numerical and experimental studies on two-phase flow of water and air is limited, it was not possible to directly validate the current two-phase results with those of other published studies. To assess the precision and consistency of the current numerical model, the air phase of the cavity was considered. The predicted Nu_{avg} were quantitatively compared with previously published experimental and numerical results, as presented in Table 2. The validation was conducted for a Pr of 0.7, Ra ranging from 10^3 to 10^7, and an inclination angle of 90°. The present results were obtained by considering only the upper half of the cavity to ensure consistency with the configurations adopted in the reference studies. The predicted Nu-Ra relationship exhibits excellent concurrence with the experimental data stated by Iyican et al. [47] and the numerical results obtained using the finite element method (FEM) by Baliga et al. [48] and the FVM by Lasfer et al. [49]. The close concurrence between the present predictions and the available experimental and numerical outcomes over an inclusive range of Ra demonstrates the accuracy and robustness of the developed numerical model.

Table 2. Comparison of the present computational results with experimental [47], and numerical outcomes from [48, 49] for the relationship between Nu_{avg} and Ra.

Ra	Iyican et al. [47] (Experimental)	Baliga et al. [48] (FEM)	Lasfer et al. [49] (FVM)	Present Study (Considering only upper half of the cavity)
10^3	–	1.50	1.66	1.56
10^4	2.20	2.30	2.33	2.31
10^5	5.20	6.00	6.09	5.99
10^6	12.50	11.80	13.40	13.10
10^7	29.52	–	–	29.21

In the earlier work of the authors' [8], the computational results were validated contrary to the benchmark solutions stated by Basak et al. [50] and Moukalled and Darwish [51]. Furthermore, the consistency of the single-phase model was reinforced in subsequent study [43] through comparison with the experimental observations of Lei et al. [3]. The simulated streamlines, isotherms, and time series of the Nu_{avg} exhibited outstanding agreement with the corresponding computational and experimental results demonstrated in [3, 50–51].

4.2. Grid dependent test

The precision and stability of numerical simulations are strongly dependent on the grid resolution and time-step size applied within the computational domain. Therefore, grid and time-step independence tests were performed at the highest Ra considered in the current study, based on the assumption that a computational setup capable of resolving the most unstable flow condition would also provide sufficient accuracy for lower Ra.

Three different grid resolutions, namely 300 × 150, 400 × 200, and 500 × 250, were examined together with two different time-step sizes of 0.01 and 0.005. Analysis of the isotherm contours revealed that the flow becomes increasingly unstable within the air phase at higher Ra. Consequently, the TTS was monitored at point P_{A2} (0, 0.065) located inside the air phase of the cavity, where the strongest flow instability was observed, for Ra = 10^8. As illustrated in Fig. 3, the calculated TTS corresponding to different grid resolutions and time-step sizes initially overlap, exhibit minor deviations during the initial transitional stage, subsequently converge closely in the fully developed regime. The obtained results show that all grid sizes and time-steps investigated are reasonably fine to adequately resolve the flow and thermal features of interest. So based on the computational efficiency and the numerical accuracy, a grid resolution of 400 × 200 and a time-step of 0.01 have been chosen for all the following simulations.

5. Results and Discussion

In this study, detailed numerical investigation has been carried out to analyze the influence of two-phase fluid flow on the transient NC, HT and E_{gen} inside a thermally stratified V-shaped cavity. The numerical analysis is conducted for two immiscible fluids, for two immiscible fluids, air with Pr of 0.71 and water with Pr of 7.01. An extensive range of Ra varying from 10^0 to 10^8, is simulated at constant AR = 1.0. The selected range of Ra is designed to encompass a wide range of buoyancy-driven HT regimes and, more importantly, to allow a systematic study of the behavior of the two-phase flow in terms of its evolution, transition and bifurcation characteristics as the buoyancy force is increased. The main aim is to investigate the dynamics of the flow development and the thermal transfer modes under different buoyancy conditions with a focus on the transition from steady two symmetric flow structures to oscillatory and chaotic developments within the two-phase flow. The transient flow structures and HT characteristics and E_{gen} behavior under various buoyancy-driven conditions are analyzed in detail in the following subsections.

5.1. Isotherms and streamlines

The evolution of isotherms and streamlines within the V-shaped cavity for an extensive range of Ra (10^3 to 10^8) at the dimensionless time τ = 3000 is illustrated in Fig. 4. For Ra values extending from 10^0 to 10^2, the flow structure exhibits negligible variation, with conduction remaining the dominant mode of HT. For brevity the results for these cases are therefore not shown. At lower Ra, the HT mechanism is predominated by conduction due to the weak buoyancy forces, resulting in a nearly stagnant fluid flow and a poor interaction between air and water phases. So, the isotherms are kept almost horizontal, suggesting a strong thermal stratification and a negligible distortion of the thermal layers. The buoyancy induced flow becomes more important with increasing Ra, which causes stronger circulation, deformation of the isotherms and more thermal mixing inside the enclosure.

Figure 4(a) presents the flow configuration for Ra = 10^3. At this condition, the flow remains essentially quiescent, and thermal conduction dominates the HT process. No significant buoyancy-driven circulation is observed in either fluid phase, and ascending or descending thermal plumes are absent. In both phases, air and water, the different thermal stratification is maintained with only small intuitions near the corners adjacent to the fluid-fluid interface.

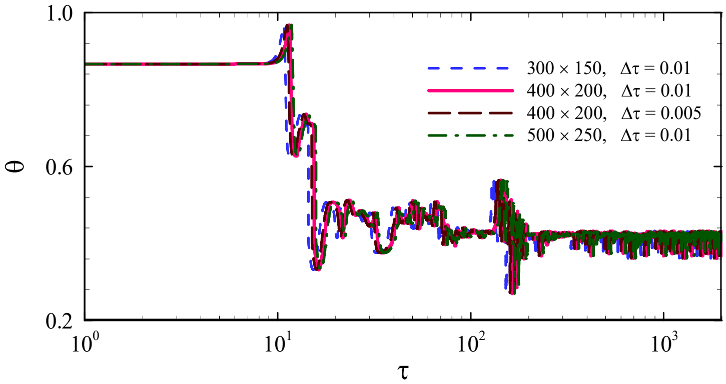

Fig. 3. Grid and time step dependence test in the air phase at point P_{A2} (0, 0.065) for Ra = 10^8.

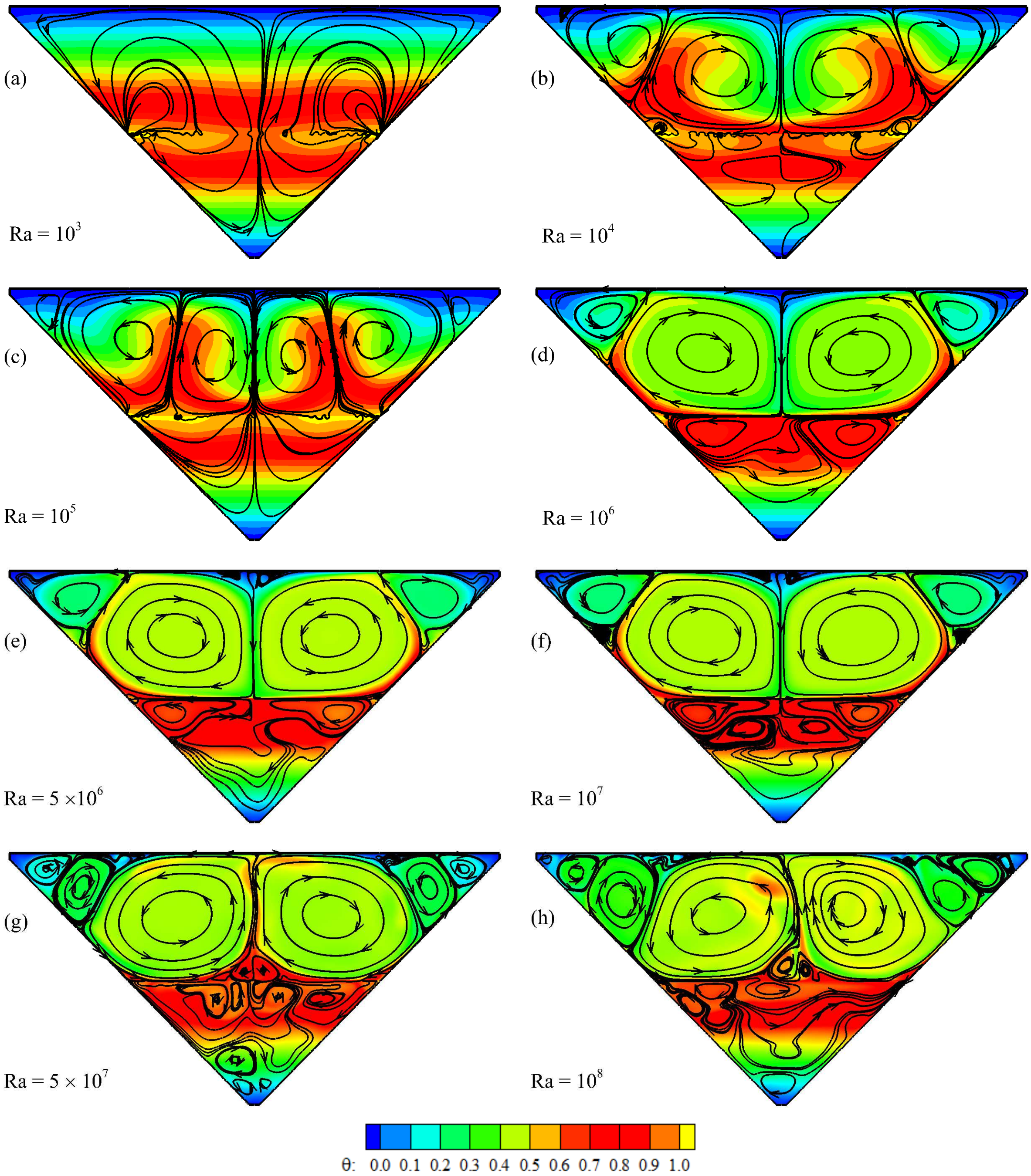

Fig. 4. Evoluation of streamlines and isotherms for various Ra at τ = 3000.

As illustrated in Fig. 4(b), when the Ra increases to 10^4, the onset of convective motion becomes. Two symmetric convective plumes emerge in the air phase, indicating the initiation of buoyancy-driven circulation. The number of convective cells increases in both phases compared with the previous case. However, conduction still remains the dominant HT mechanism, and the flow field preserves symmetry about the perpendicular centerline, suggesting a balanced development of buoyancy forces. As portrayed in Fig. 4(c), with a further upsurge to Ra = 10^5, the convective motion becomes notably more vigorous with an increase in the size and number of circulation cells in the air and water phases. While thermal stratification exists, it gradually diminishes due to increased fluid motion and increased thermal mixing in the enclosure.

A significant change in the flow structure is displayed in Fig. 4(d) at Ra = 10^6. Thermal stratification completely vanishes at the air phase, suggesting that the convective transport dominated by HT mechanism. During the transitional stage, oscillatory behavior of the air-phase flow is observed and finally, at τ = 3000, the steady state is attained. The thermal stratification, on the other hand, is partially maintained in the water phase, because of the relatively slow thermal response and high viscous effect of the water phase, with the higher Pr fluid. In Fig. 4(e), corresponding to Ra = 5 × 10^6, the flow structure becomes increasingly complex. In both phases more convective cells develop and the circulation becomes noticeably stronger. The air phase displays vigorous convection with distributed vortical structures, whereas stratification still persists in the water phase, although its influence becomes weaker than that observed at lower Ra.

As the Ra rises, the buoyancy force becomes more important, and the thermal plumes become stronger and convective transport increases. The interaction between the rising hot fluid and downward cold fluid progressively destabilizes the initially stable flow configuration in the air phase. Figure 4(f) demonstrates the flow behavior at Ra = 10^7. At this stage, two additional small vortices emerge near the upper boundary of the air phase. The principal cells of circulation have a rhythmic rotational motion. Therefore, the flow in the air-phase has entered a periodic regime at τ = 3000. Meanwhile, thermal stratification begins to deteriorate adjacent to the upper region of the water phase due to intensified convective mixing, whereas the lower region remains comparatively stratified. However, the overall streamline topology remains relatively unchanged compared with the earlier case. For Ra = 5 × 10^7, as portrayed in Fig. 4(g), the flow dynamics in the air phase gets complicated. A new small vortex is also generated just above the fluid interface, which makes the flow more unstable and complicated. Conversely, the rotational motion in the water phase is relatively poor, so the convective circulation in the lower fluid phase is relatively weak. Finally, the flow characteristics at Ra = 10^8 is showed in Fig. 4(h). At this high Ra, the air phase exhibits very irregular and asymmetric vortex structures, indicating the onset of chaotic convection. At the same time, the water phase shows a weak oscillatory motion.

5.2. Asymmetric flow

To examine the alteration from symmetric to asymmetric flow behavior within the V-shaped cavity, TTS were examined at two geometrically symmetrical points in both the phases. In the air phase, the observation points were selected as P_{A3} (0.30, 0.065) and P_{A4} (-0.30, 0.065), whereas in the water phase, the corresponding symmetric points were P_{W2} (0.30, -0.065) and P_{W3} (-0.30, -0.065). As shown in Fig. 5(a), for Ra = 9 × 10^5, the TTS curves at each pair of symmetric points in both the air and water phases exhibit complete overlap throughout the simulation period. This identical TTS confirm that the flow structure remains perfectly symmetric with regards to the cavity's centerline. However, a notable change in the flow behavior is observed when the Ra increases to 10^6, as presented in Fig. 5(b). At the initial stage, the TTS at the symmetric locations remain nearly identical, indicating that the flow initially develops in a symmetric manner. Gradually the TTS begin to deviate from one another as the dimensionless time τ goes up. The deviation is seen earlier in the air phase (τ = 33) than in the water phase (τ = 85). This separation reveals that the thermal symmetry has been collapse and the asymmetric flow behavior inside the cavity has begun. The air phase develops asymmetric flow structures earlier and more prominently due to the lower density and the higher sensitivity to buoyancy-induced disturbances. The water phase, on the other hand, shows delayed asymmetry because of its larger thermal inertia and stronger stratification effects. Therefore, Ra = 10^6 is found to be the critical Ra at which the symmetric flow state loses its stability, leading to the symmetry-breaking transition as a pitchfork bifurcation in the present two-phase V-shaped cavity.

5.3. Route to unsteady flow

To analyze the evolution of unsteady flow behavior within the V-shaped cavity, the TTS were monitored at point P_{W1} (0, -0.034) in the water phase and point P_{A1} (0, 0.034) in the air phase, for different Ra, as illustrated in Fig. 6. At Ra = 10^6, the TTS in the water phase shows a single downward oscillation in the early transitional stage before gradually reaching a steady-state condition. Initially in the air phase, few oscillations of small amplitude are observed, indicating the presence of weak transient instabilities due to buoyancy-driven motion. However, these oscillations decay with time and the flow finally attains a steady state for the range 900 ≤ τ ≤ 3000. The flow behavior is much more dynamic at Ra = 5 × 10^6. In the water phase, the TTS displays two upward oscillations, showing an increase in thermal instability and convective activity.

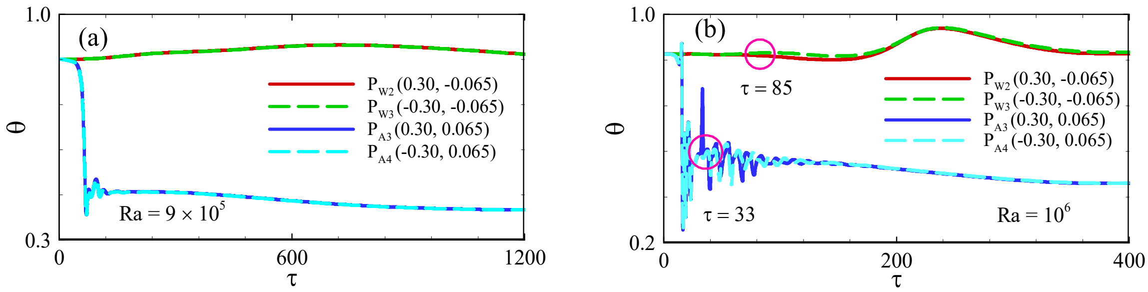

Fig. 5. Asymmetry test in the air and water phase for the geometrically symmetric points along the y-axis.

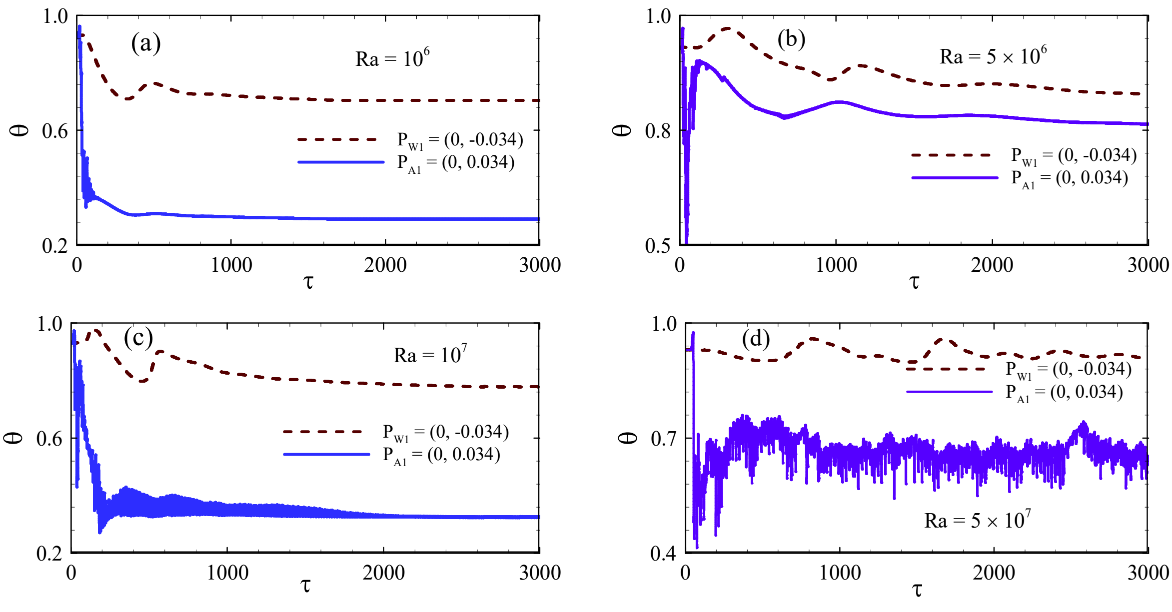

Fig. 6. Transition from asymmetric steady state to unsteady state for the different Ra.

Simultaneously, the air phase exhibits a greater number of oscillations during the transitional period. The oscillations do not completely decay, and the flow demonstrates weak oscillatory behavior throughout the interval $1200 \le \tau \le 3000$. For Ra = 10^7, in the water phase two upward oscillations are again detected; however, the wavelength of the oscillations becomes significantly shorter compared with the lower Ra case. In the air phase, the oscillatory behavior becomes substantially more pronounced throughout the transitional stage. With time progresses, the TTS develops a regular periodic pattern, demonstrating the onset of self-sustained thermal oscillations. The flow may subsequently undergo a Hopf bifurcation. At Ra = 5×10^7, the oscillatory dynamics intensify further in both fluid phases. The water phase shows relatively stronger and increasingly irregular temperature fluctuations which indicates the amplification of thermal instabilities. In the air phase, the previously periodic oscillations lose their regularity and evolve into highly irregular temporal variations. This behavior confirms the changeover from periodic to chaotic flow. Thus, the observed alteration from steady to periodic and chaotic states is physically associated with the progressive dominance of buoyancy forces, increasing thermal-gradient strength, and nonlinear interactions between the thermal and hydrodynamic fields.

To gain deeper understanding into the flow dynamics, consider TTS in the interval τ = 2900 to 3000 were analyzed for different Ra values for both phases, as illustrated in Fig. 7. In the air phase, at point P_{A1} (0, 0.034), for the Ra value of 5×10^6, the flow remains constant over time, i.e., the flow becomes steady state, as portrayed in Fig. 7(a). When the Ra increases to 10^7, the flow undergoes an alteration from steady to periodic oscillatory state with regular temperature fluctuations, as presented in Fig. 7(b). At Ra = 5×10^7, the oscillations become irregular and non-repeating, which is the onset of chaotic flow behavior in the air phase, as depicted in Fig. 7(c). In contrast, the water phase at point P_{W1} (0, 0.034), exhibits a comparatively different trend. For all investigated Ra ranging from 5×10^6 to 5×10^7, the TTS fluctuates over time, as demonstrated in Fig. 7(d-f).

Unlike the air phase, the oscillatory characteristics in the water phase remain relatively moderate, although small-amplitude fluctuations become noticeable at Ra = 5×10^7 as illustrated in Fig. 7(f). These results suggest that the water phase requires higher Ra and longer time evolution to show clear transitions in flow behavior than the air phase. The different flow dynamics are mainly because of the difference in their thermophysical properties, especially Pr. Air, which has a relatively low Pr, has comparatively higher thermal diffusivity, which allows thermal disturbances to diffuse more quickly through the fluid. This may promote larger thermal structures and stronger coupling between temperature fluctuations and the flow field around them. Water, however, has a much larger Pr and therefore a lower thermal diffusivity relative to its momentum diffusivity. Hence the thermal disturbances are more confined and the thermal boundary layers are relatively thinner. These differences influence the development and interaction of buoyancy-driven structures in the two phases, resulting in different transition characteristics and degrees of temporal instability.

To understand better the changeover in the air phase from a steady to a chaotic regime, the phase-space trajectories in the u-θ plane at point P_{A3} (0.30, 0.065) over the time interval τ = 800 to 2500, as demonstrated in Fig. 8. In Fig. 8(a) the blue rounded point shows that, for Ra = 5×10^6, the trajectory gradually converges to a single stable fixed point. The collapse of the trajectory into a stationary equilibrium state justifies that the flow reaches a steady-state condition at approximately τ = 2500. As the Ra increases to 10^7, the flow dynamics undergo a significant transition, as illustrated in Fig. 8(b). The phase-space trajectory does not converge to a fixed point, but rather forms a closed loop, a characteristic of a stable limit cycle. This periodic orbit marks the beginning of the appearance of self-sustaining oscillations in the system. Such a changeover from a stable equilibrium state to periodic flow strongly recommends the occurrence of a Hopf bifurcation in the range $5 \times 10^6 < \text{Ra} \le 10^7$. The flow structure in Fig. 8(c) is significantly different when Ra is further increased to 5×10^7. Instead of a closed cycle, the trajectory now shows an irregular, non-repeating path, which indicates the onset of chaotic flow behavior.

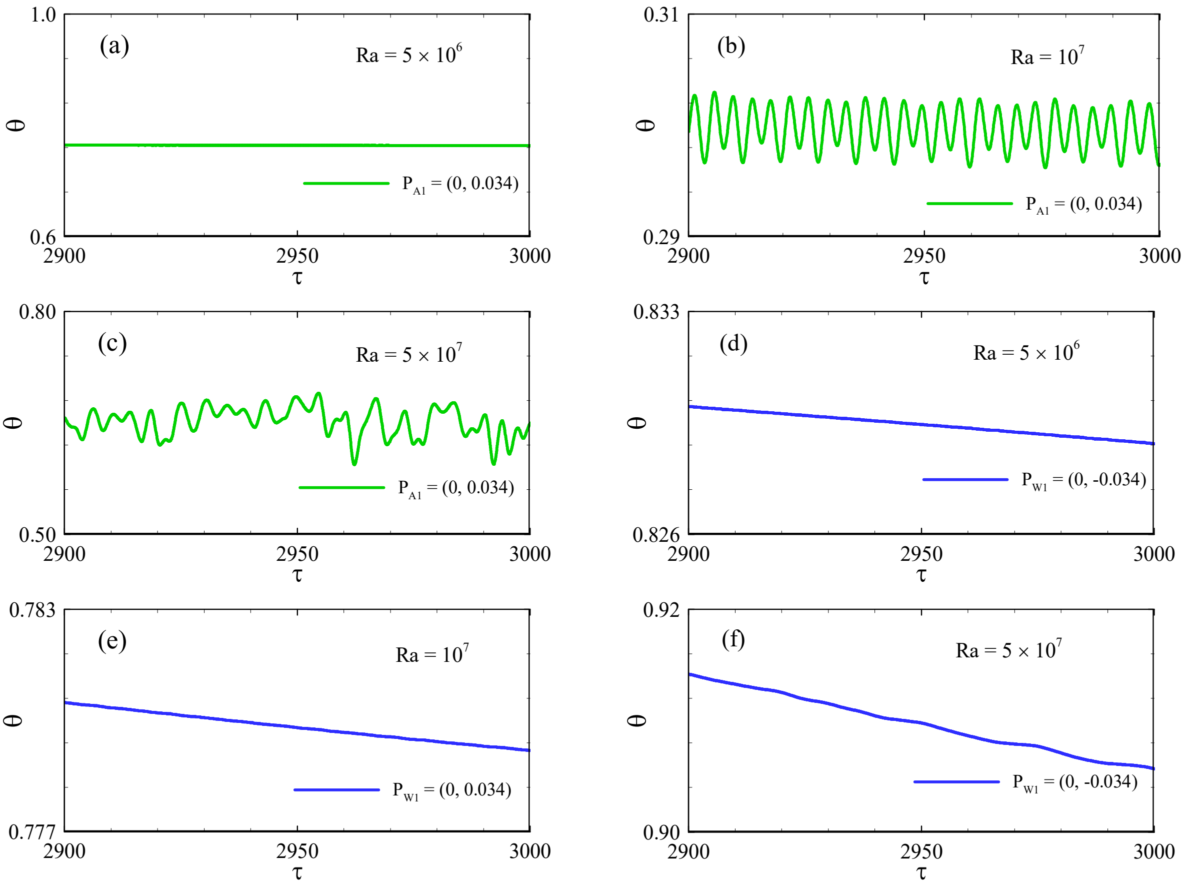

Fig. 7. Temperature time series: (a-c) in the air phase at point P_{A1} (0, 0.034) and (d-f) in the water phase at point P_{W1} (0, - 0.034).

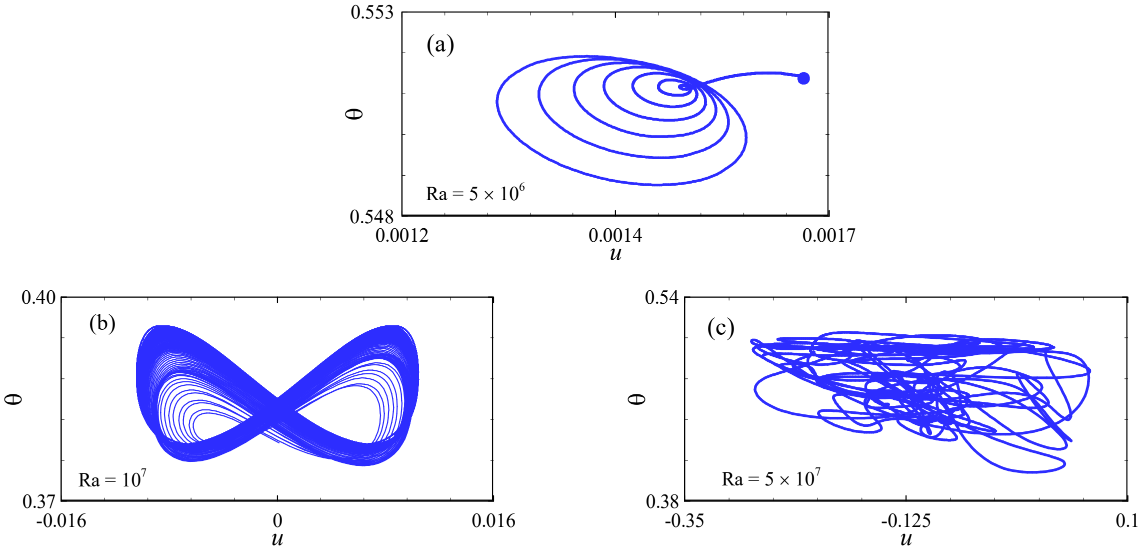

Fig. 8. Limit point and limit cycles in the air phase at point P_{A3} (0.30, 0.065) for the different Ra.

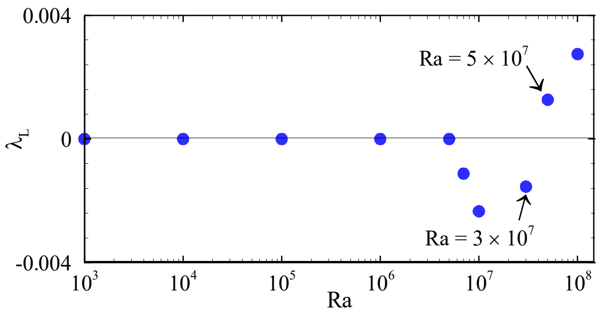

Fig. 9. Variation of λ_L with Ra, illustrating the shift from steady to chaotic flow in the air phase.

In the air phase, the largest Lyapunov exponent (λ_L) is a quantitative indicator of the shift from steady to chaotic behavior in buoyancy-driven flows. This parameter evaluates the sensitivity of the system to initially nearby trajectories in phase space and characterizes the onset of chaotic flow. Specifically, if ε_0 denotes the initial separation between two trajectories and $\varepsilon(\tau)$ represents their separation after a time interval τ, the evolution can be expressed as [52]:

$$\varepsilon(\tau) \approx \varepsilon_0 e^{\lambda_L \tau}, \tag{18}$$

where a positive value of λ_L indicates exponential divergence and hence chaotic dynamics. The λ_L is computed as:

$$\lambda_L = \frac{1}{\tau_n - \tau_0} \sum_{j=1}^{n} \ln\left(\frac{\varepsilon(u_j)}{\varepsilon(u_{j-1})} \right). \tag{19}$$

where $\varepsilon(u_j)$ denotes the Euclidean distance between u_j and u_{j-1}, τ_0 is the initial time (τ_0 = 2500), and τ_n corresponds to the final time after n iterations (τ_n = 3000 with n = 40000).

The computed values of λ_L for different Ra, which provide clear insight into the dynamical behavior of the system in the air phase, shown in Fig. 9. For Ra ≤ 5 × 10^6, the computed values λ_L is approximately zero ($\lambda_L \approx 0$), indicating a steady-state flow regime characterized by the absence of sensitive dependence on initial conditions. This result is consistent with the symmetric and steady flow structures discussed above. As the Ra increased within the range 5 × 10^6 < Ra ≤ 4 × 10^7, the value of λ_L is negative, suggesting that the flow becomes oscillatory. With a further rise of Ra, there is a dramatic change in the dynamics of the system. At Ra = 5 × 10^7, the λ_L becomes positive (λ_L = 0.001267), confirming the onset of chaos. This change is well correlated with the flow patterns shown in Figs. 7 and 8, where the steady, periodic, and chaotic flow structures were observed in the air phase. Moreover, with the increase of Ra, λ_L also increases, which means the chaotic phenomenon of the air phase keeps strengthening.

5.4. Heat transfer

The HT characteristics within the two-phase cavity are analyzed in terms of the $[Nu_{avg}]_i$, along the sloped walls in both the air and water phases. The temporal evolution of $[Nu_{avg}]_i$ for different Ra are shown in Fig. 10. Viscous force dominates the buoyancy force in the case of relatively low Ra (≤ 10^5), and HT is mainly dominated by conduction. Beyond this threshold, buoyancy forces become predominant in the air phase. Thus, the primary mode of HT is shifts from conduction to convection, leading to an increase in HT rate with higher Ra. From the time series of $[Nu_{avg}]_i$ at the sloped wall for Ra = 10^6, the oscillations are not very noticeable in the water phase than the air phase. As Ra is increased further, the HT rate in the air phase also increases as seen by the increase of $[Nu_{avg}]_i$, in Fig. 10(a). However, the water phase shows a much different trend the HT rate is relatively low due to the much higher viscosity and thermal inertia of water. The value of $[Nu_{avg}]_i$ in the water decreases with time after some transitional period as depicted in Fig.10(b), indicating that convective contribution decreases with time. It has been proposed that this behavior is due to the stabilizing effect of the high viscosity and thermal inertia of water that inhibit the growth of large-scale convective structures. In summary, the HT characteristics in the two-phase cavity are very phase dependent. For higher Ra, the convective HT of the air phase is strong, and dynamic, whereas the water phase is conduction dominated with very little convection over a longer period.

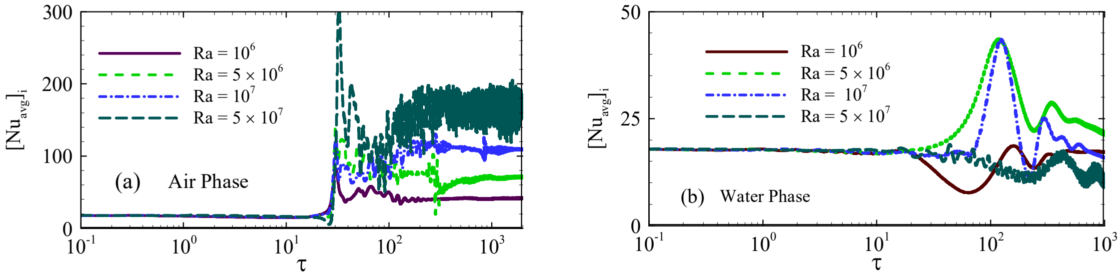

Fig. 10. Time series of $[Nu_{avg}]_i$ for the different Ra: (a) at the inclined wall in the air phase and (b) at the inclined wall in the water phase.

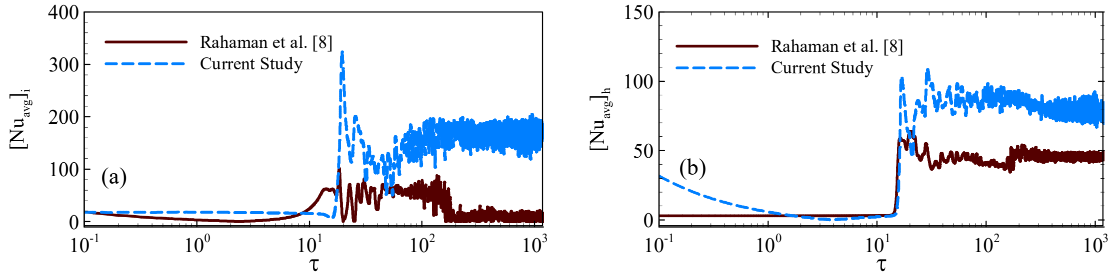

Fig. 11. Nu_{avg} time series for the air in the single-phase and two-phase cases for Ra = 4 × 10^7: (a) at the inclined wall $[Nu_{avg}]_i$ and (b) at the top horizontal wall $[Nu_{avg}]_h$.

5.5. Comparison of heat transfer for air in the single-phase and two-phase cases

A comparative analysis was carried out with the previous two-phase simulation and the earlier single-phase simulation by the authors [8] which was based on convective flow inside a trapezoidal cavity filled only with stratified air. For the sake of comparison, the geometric parameters, such as sloped wall sizes, top wall sizes and the thermal boundary conditions applied on the air domain were kept the same as in [8]. The main difference is the fluid configuration: In the previous study, a single-phase air system was investigated, whereas in the present work, a two-phase system, with the lower part of the cavity filled with stratified water and the upper part with stratified air, has been investigated. The comparisons of the HT performance of the two configurations in terms of the Nu_{avg} along the inclined wall $[Nu_{avg}]_i$ (Fig. 11(a)) and the top horizontal wall $[Nu_{avg}]_h$ (Fig. 11(b)) in the air phase are shown in Fig. 11. It is evident from the results that the two-phase system clearly has much better HT performance in comparison to the single-phase case. The augmentation is primarily due to the high viscosity ratio air-water which increases the shear at the interface and thereby further increases the convective transport of the airside. These results indicate the importance of the dynamics of the interface in the governing multiphase NC, and the distinct advantage of the two-phase system over the single-phase one with respect to HT.

5.6. Entropy generation

The spatial distribution of local E_{gen} arising from HT irreversibility (E_{ht}) and FF irreversibility (E_{ff}) for Ra = 10^6, 5 × 10^6, 10^7 and 5 × 10^7 are shown in Fig. 12. The fluid motion is weak and the flow is mostly conduction dominated at small Ra. Thus, temperature gradients are the main source of E_{gen}, but the effect of viscous dissipation is relatively small due to the low velocities of the fluids. So, in the low Ra regime the total E_{gen} is primarily influenced by thermal irreversibility, especially in the areas of high temperature gradient close to the heated and cooled surfaces. With an increasing Ra, buoyancy-induced motion increasingly dominates resulting in increasing fluid velocities, increasing recirculation, and increasing velocity gradients. Therefore, the contribution of the viscous friction to the overall E_{gen} increases.

At Ra = 10^6, the distribution shows that, the local E_{gen} is mainly dominated by HT and the E_{gen} due to FF is insignificant. This behavior indicates that HT within the enclosure is mainly conduction dominated at lower buoyancy strengths. As the Ra increases, buoyancy-induced motion becomes progressively stronger, leading to enhanced velocity gradients and a corresponding increase in E_{gen} due to FF. Consequently, at Ra = 5 × 10^7, the contribution of E_{ff} becomes considerably more pronounced, particularly within the air phase where vigorous circulation develops. Thus, the FF irreversibility becomes the leading contributor of E_{gen} in the air phase.

The distributions also show that E_{gen} due to HT is strong near the heated and cooled boundaries, where temperature gradients are maximum. In contrast, E_{gen} associated with FF is localized in regions characterized by strong velocity gradients and vortex activity. The increase of Ra enhances the convective motion in the air phase, thus amplifying thermal and hydrodynamic irreversibilities. The results of the streamline and isotherm reveal that the buoyancy driven flow becomes more significant with the higher Ra which will definitely alters the E_{gen} pattern inside the cavity.

In the water phase, the measured thermal and flow properties are quite different than those in the air phase. The upper interface of the water phase was heated, while the sloped walls were thermally stratified from interface to bottom and the bottom wall is cooled. This thermal configuration suppresses buoyancy-driven circulation inside the water phase, resulting in relatively weak fluid motion. As evidenced by the streamline and isotherm contours, only minor variations in velocity and temperature are observed in the water phase for all Ra considered.

The E_{gen} in the water phase of the cavity is lower than that in the air phase, mainly because of the differences in their thermophysical properties and the resulting HT and flow behavior. Water has a considerably higher thermal conductivity than air, which facilitates more effective heat diffusion and produces a more consistent temperature distribution in the water phase of the cavity. So, the temperature gradients associated with thermal irreversibility are reduced, which leads to lower E_{gen} due to HT. Furthermore, the higher Pr of water promotes stronger thermal diffusion characteristics, while its higher viscosity suppresses excessive velocity gradients and reduces the associated FF irreversibility. Hence, E_{gen} in the water phase is almost completely dominated by HT irreversibility, while the contribution of FF irreversibility is negligible. This result suggests that HT within the water phase is mainly conduction controlled and that the viscous effects dominating over buoyancy-induced motion. The dominance of thermal irreversibility in the water phase is also consistent with the relatively higher values of the Be_{avg}, indicating the strong influence of conductive HT on the overall E_{gen} process.

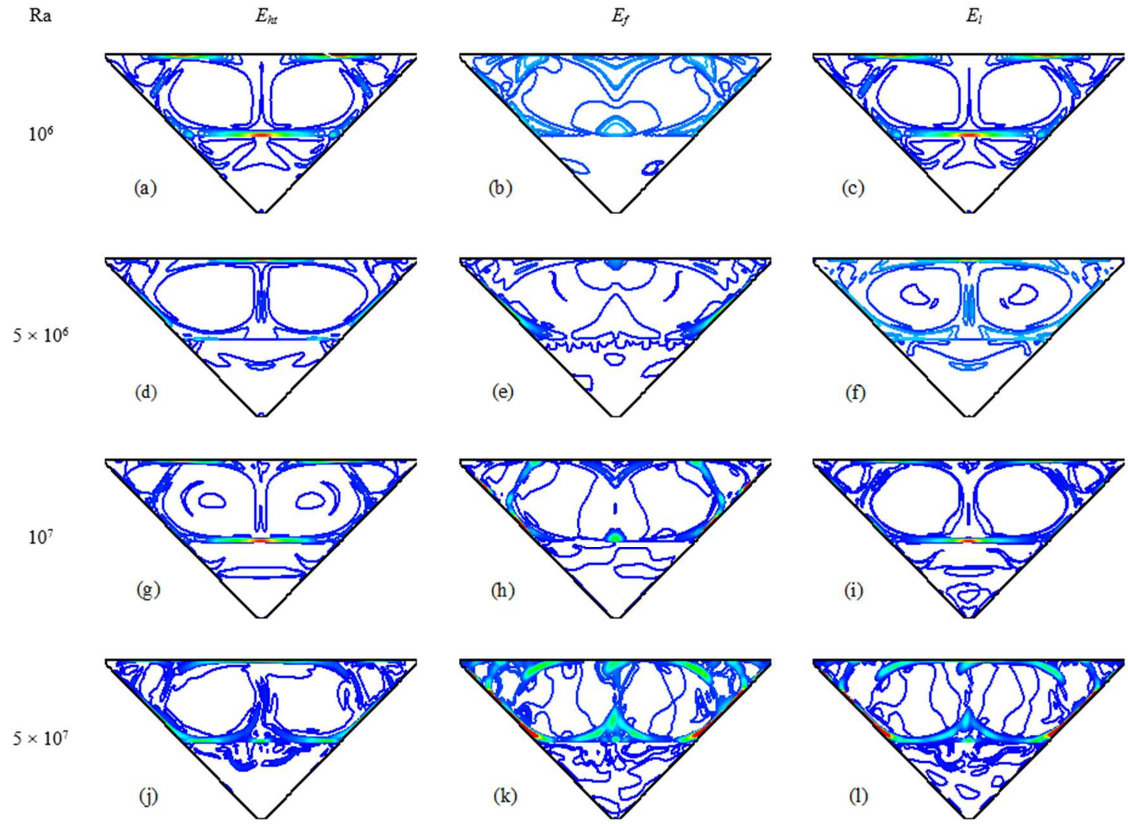

Fig. 12. Distribution of E_{gen} for diverse Ra values: the second column displayed the E_{gen} due to HT (E_{ht}), the third column shown the E_{gen} due to FF (E_{ff}), and the fourth column presented the local E_{gen} (E_l).

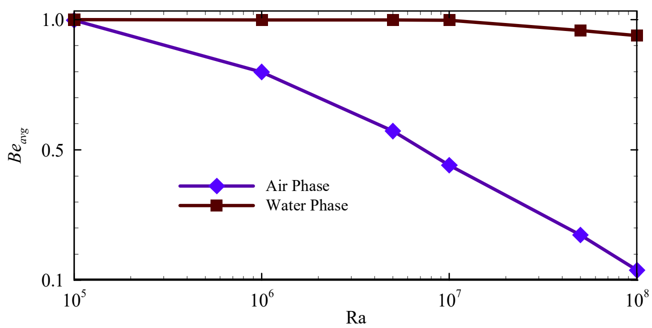

Fig. 13. Average Bejan number variation in the air and water phases for the different Ra.

Figure 13 illustrates the disparity of the Be_{avg} with Ra for the air and water phases. For Ra ≤ 10^5, Be_{avg} is very close to one in both phases, indicating that E_{gen} is almost entirely dominated by HT irreversibility, while the contribution of FF irreversibility is negligible. This behavior verifies that the transport mechanism is almost conduction controlled with only weak fluid motion within the cavity at low buoyancy forces. A general trend of decreasing Be_{avg} with increasing Ra values is observed in the air phase. The highest value of Be_{avg} ($Be_{avg,\ \max} \approx 1$) occurs at Ra = 10^5, it further highlights the effect of thermal irreversibility under weak convective conditions. But the buoyancy-driven circulation in the air region is much more vigorous for increasing Ra, leading to large velocity gradients and large viscous dissipation. Thus, the FF irreversibility effect becomes more and more pronounced, and Be_{avg} starts to diminish and reach its lowest value at Ra = 10^8. This tendency clearly suggests the shift from the conduction dominated HT to regime where the hydrodynamic irreversibilities become increasingly prominent. In contrast, the water phase maintains comparatively higher values of Be_{avg} throughout the investigated Ra range. The persistent high value of Be_{avg} suggests that HT irreversibility remains the principal contributor to E_{gen} within the water phase. This phenomenon can be attributed to the suppression of buoyancy-induced flow by viscous resistance and thermal stratification effects. Therefore, the fluid motion in the water phase is still quite weak and E_{gen} continues to be governed by conductive HT rather than viscous dissipation. The observed differences between the air and water phases underline the different thermal and hydrodynamic behavior of the two fluids, and highlight the stronger influence of the convection-induced irreversibilities for the air phase at higher Ra.

6. Conclusions

In practical engineering systems, NC flows often occur in transient conditions with complicated thermal interactions among multiple phases of fluid. The VOF approach is used to perform a numerical study of the transient NC, HT, and related E_{gen} within a V-shaped cavity filled with two stratified fluids. The combined analysis of streamline and isotherm contours, Nu_{avg} analyses and E_{gen} resulting from HT and FF irreversibilities, has provided valuable insight into the underlying flow physics. The numerical scheme based on FVM and the VOF model showed good performance in accurately capturing the thermal fluctuations, the flow transitions and the interfacial behaviors between the two phases. The key results of the present investigation are briefly outlined as follows:

- The isotherm and streamline distributions show complex flow patterns which are controlled by both thermal and geometrical factors and provide detailed picture of the fluid flow and HT mechanisms inside the cavity.
- HT in both phases was mainly conduction dominated for Ra ≤ 10^5, whereas a changeover from symmetric to asymmetric flow behavior was encountered at Ra = 10^6.
- The air phase exhibited periodic oscillatory behaviour at Ra = 10^7. The water phase continued to have relatively weak circulation due to suppressed buoyancy effects.
- For Ra = 5 × 10^7, chaotic flow behavior was observed in the air phase while the water phase showed weak rotational motion with limited thermal disturbance.
- The two-phase configuration significantly enhanced the total HT performance in particular in the air phase, due to the higher interfacial convective transport compared to the single-phase case.
- The E_{gen} analysis demonstrates the importance of irreversibility in such systems. For Ra < 10^6, the E_{gen} is mainly controlled by HT, while for Ra = 10^6, the buoyancy effects in the air phase become larger than the viscous resistance. For Ra > 10^7, fluid friction irreversibility in the air phase was found to become more important, while its contribution was still negligible in the water phase due to the persistence of weak fluid motion.
- The Be_{avg} decreased with increasing Ra in the air phase indicating a gradual shift of the irreversibility to FF-dominated at higher buoyancy strengths. Conversely, the water phase showed a relatively higher Be_{avg}, indicating the dominance of HT irreversibility related to conductive transport.

To summarize, the present research contributes to the knowledge of the transient two-phase NC flow and E_{gen} in stratified cavities. The obtained findings give useful understandings for the design and optimization of thermal systems with multiphase convection.

7. Limitations and Future Work

The present study gives good knowledge about transient NC, HT, and E_{gen} occurring in a two-phase stratified V-shaped cavity. Nevertheless, some limitations should be considered when interpreting the results. Firstly, the analysis was carried out in 2D domain, and many practical thermal systems have inherent 3D flow structure and HT mechanisms. Second, the fluids were to be Newtonian, incompressible, immiscible and having constant thermophysical properties. The influence of surface tension, phase change phenomena and interfacial mass transfer has also been ignored in the present model. In addition, the study was limited to a narrow range of Ra and no attempt was made to experimentally verify the flow regimes predicted to be oscillatory and chaotic.

These limitations could be addressed in future work by extending the analysis to 3D domains and by considering a wider range of cavity geometries. Inclusion of other fluid pairs and temperature dependent thermophysical properties would provide a more comprehensive picture of multiphase convection. The physical realism of the model would be further improved by including surface tension, evaporation-condensation mechanisms and interfacial mass transfer.

Author Contributions

M.M. Rahaman conceptualized the study, developed the methodology, conducted the investigation, performed the visualization, curated the data, and wrote the original draft; S. Bhowmick conceptualized the study, supervised the work, and contributed to writing – review and editing; G. Saha contributed to writing – review and editing; S.C. Saha supervised the work and contributed to writing – review and editing. The manuscript was written through the contribution of all authors. All authors discussed the results, reviewed, and approved the final version of the manuscript.

Acknowledgments

Not applicable.

Conflict of Interest

The authors affirm that they have no conflict of interests concerning the research and publication of this article.

Funding

The authors received no financial support for the research.

Data Availability Statements

The data supporting the findings of this study are available from the corresponding author upon reasonable request.

Nomenclature

AR	Aspect ratio, H/L	T_c	Temperature at the top and bottom walls [K]
Be	Bejan number	T_h	Temperature at the interface [K]
Be_{avg}	Average Bejan number	T_∞	Environmental temperature [K]
Be_l	Local Bejan number	ΔT	Temperature difference, (T_h - T_c) [K]
Cp	Specific heat [J/kg.K]	U, V	Velocity [m/s]
E_{ff}	Entropy generation due to FF	u, v	Dimensionless velocity
E_{gen}	Entropy generation	X, Y	Coordinates
E_{ht}	Entropy generation due to HT	x, y	Dimensionless coordinates

E_l	Local entropy generation
F_s	Force caused by surface tension [N/m]
f_s	Dimensionless force caused by surface tension
g	Gravitational force [m/s^2]
H, L	Height and length and of the cavity [m]
k	Thermal conductivity [W/(m·K)]
l	Dimensionless length of the sloped walls
n	Dimensionless coordinate normal to the sloped walls
Nu_{avg}	Average Nusselt number
P	Pressure [N/m^2]
p	Dimensionless pressure
Pr	Prandtl number, ν/κ
Ra	Rayleigh number, $g\beta(T_h\text{-}T_c)H^3/\nu\kappa$
s	Dimensionless coordinate along the sloped walls
T	Temperature [K]
t	Time [s]

Greek symbols

α	Volume fraction
β	Thermal expansion coefficient [1/K]
θ	Dimensionless temperature
θ_c	Dimensionless temperature at the top and bottom walls
θ_h	Dimensionless temperature at the interface
θ_i	Dimensionless temperature at the sloped walls
τ	Dimensionless time
$\Delta\tau$	Dimensionless time step
κ	Thermal diffusivity [m^2/s]
λ_L	Largest Lyapunov exponent
μ	Dynamic viscosity [kg/ms]
ψ	Irreversibility distribution ratio
ν	Kinematic viscosity [m^2/s]
ρ	Density [kg/m^3]
σ	Surface tension [N/m]

References

[1] Patterson, J., Imberger, J., Unsteady natural convection in a rectangular cavity, *Journal of Fluid Mechanics*, 100(1), 1980, 65–86.

[2] Lin, W., Armfield, S. W., Patterson, J. C., Unsteady natural convection boundary-layer flow of a linearly-stratified fluid with Pr < 1 on an evenly heated semi-infinite vertical plate, *International Journal of Heat and Mass Transfer*, 51(1), 2008, 327–343.

[3] Lei, C., Armfield, S. W., Patterson, J. C., Unsteady natural convection in a water-filled isosceles triangular enclosure heated from below, *International Journal of Heat and Mass Transfer*, 51(11), 2008, 2637–2650.

[4] Shaon, S. M. H., Rahaman, M. M., Unsteady natural convection and heat transfer analysis within a thermally stratified air-filled square enclosure, *Mathematics and Mechanics of Complex Systems*, 14(1), 2025, 37-57.

[5] Hossain, M. N., Shaon, S. M. H., Rahaman, M. M., Transient Natural Convection and Entropy Generation Analysis in a Stratified Square Enclosure, *AUT Journal of Mechanical Engineering*, 10(2), 2026, 153-166.

[6] Shaon, S. M. H., Rahaman, M. M., Saha, S. C., Bhowmick, S., Comparative Analysis of Unsteady Natural Convection and Thermal Performance in Rectangular and Square Cavities Filled with Stratified Air, *Fluids*, 11(2), 2026, 33.

[7] Bhowmick, S., Xu, F., Zhang, X., Saha, S. C., Natural convection and heat transfer in a valley shaped cavity filled with initially stratified water, *International Journal of Thermal Sciences*, 128, 2018, 59–69.

[8] Rahaman, M. M., Bhowmick, S., Pada Ghosh, B., Xu, F., Nath Mondal, R., Saha, S. C., Transient natural convection flows and heat transfer in a thermally stratified air-filled trapezoidal cavity, *Thermal Science and Engineering Progress*, 47, 2024, 102377.

[9] Hanafizadeh, P., Saidi, M. H., Nouri Gheimasi, A., Ghanbarzadeh, S., Experimental investigation of air-water, two phase flow regimes in vertical mini pipe, *Scientia Iranica*, 18(4), 2011, 923-929.

[10] Zhang, J., Huang, N., Lei, L., Liang, F., Wang, X., Wu, Z., Studies of gas-liquid two-phase flows in horizontal mini tubes using 3D reconstruction and numerical methods, *International Journal of Multiphase Flow*, 133, 2020, 103456.

[11] Talley, J. D., Worosz, T., Kim, S., Buchanan Jr, J. R., Characterization of horizontal air–water two-phase flow in a round pipe part I: Flow visualization, *International Journal of Multiphase Flow*, 76, 2015, 212-222.

[12] Dassler, C., Janoske, U., Experimental investigation of single-and two-phase pressure drop in slender rectangular 180° return bends, *Experimental Thermal and Fluid Science*, 103, 2019,126-132.

[13] Zahedi, R., Rad, A. B., Numerical and experimental simulation of gas-liquid two-phase flow in 90-degree elbow, *Alexandria Engineering Journal*, 61(3), 2022, 2536-2550.

[14] Kükrer, E., Eskin, N., Experimental assessment of local void fraction and flow development in a U-bend piping system for air-water two-phase flow, *International Journal of Multiphase Flow*, 169, 2023, 104610.

[15] Yaqop, B. N., Gas-liquid two-phase flow pressure drop in flattened tubes: an experimental and numerical study, *Journal of Thermal Engineering*, 10(1), 2021, 196-206.

[16] Yin, B., Zhang, C., Ding, T., Chen, C., Feng, K., Wang, Z., Sun, B., An experimental and numerical study of gas-liquid two-phase flow moving upward vertically in larger annulus, *Engineering Applications of Computational Fluid Mechanics*, 19(1), 2025, 2476605.

[17] Lv, W., Shi, M., Chen, P., Dai, J., Chen, H., Experimental and numerical studies on the characteristics and mechanisms of convective heat transfer in gas–liquid two-phase flows, *International Journal of Heat and Fluid Flow*, 118, 2026, 110209.

[18] Huang, G., Han, J., Shan, L., Li, W., The impacts of gas-liquid two-phase flow regimes on heat transfer performance and pressure drop in microchannels-an experimental study, *International Journal of Thermal Sciences*, 219, 2026, 110232.

[19] Li, W., Yang, F., Alam, T., Khan, J., Li, C., Experimental and theoretical studies of critical heat flux of flow boiling in microchannels with microbubble-excited high-frequency two-phase oscillations, *International Journal of Heat and Mass Transfer*, 88, 2015, 368-378.

[20] Tiwari, N., Moharana, M.K., Conjugate heat transfer analysis of liquid-vapor two phase flow in a microtube: A numerical investigation, *International Journal of Heat and Mass Transfer*, 142, 2019,118427.

[21] Nishio, J., Kurose, R., Numerical simulation of gas–liquid two-phase flow in a horizontal manifold with downward branches, *Journal of Fluid Science and Technology*, 19(1), 2024, JFST0002-JFST0002.

[22] Zhang, Y., He, C., Li, P., Numerical investigation of gas-liquid two-phase flow in horizontal pipe with orifice plate, *Progress in Nuclear Energy*, 138, 2021, 103801.

[23] Sheng, L., Chang, Y., Wang, J., Deng, J., Luo, G., Hydrodynamics of gas–liquid microfluidics: A review, *Chemical Engineering Science*, 285, 2024, 119563.

[24] Parvareh, A., Rahimi, M., Alizadehdakhel, A., Alsairafi, A. A., CFD and ERT investigations on two-phase flow regimes in vertical and horizontal tubes, *International Communications in Heat and Mass Transfer*, 37(3), 2010, 304–311.

[25] Deendarlianto, Andrianto, M., Widyaparaga, A., Dinaryanto, O., CFD Studies on the gas-liquid plug two-phase flow in a horizontal pipe, *Journal of Petroleum Science & Engineering*, 147, 2016, 779–787.

[26] López, J., Pineda, H., Bello, D., Ratkovich, N., Study of liquid–gas two-phase flow in horizontal pipes using high speed filming and computational fluid dynamics, *Experimental Thermal and Fluid Science*, 76, 2016, 126–134.

[27] Georgoulas, A., Andredaki, M., Marengo, M., An enhanced VOF method coupled with heat transfer and phase change to characterise bubble detachment in saturated pool boiling, *Energies*, 10(3), 2017. 272.

[28] Shi, X., Zheng, K., Yin, B., Numerical method for gas-liquid two-phase flow with phase change heat transfer considering compressibility using OpenFOAM, *International Journal of Thermal Sciences*, 188, 2023, 108195.

[29] Xiaoqi, M. A., Yueshe, W. A., Jiaming, T. I., Numerical investigation on characteristics of interfacial wave of liquid film in gas–liquid two-phase flow using OpenFOAM, *Chinese Journal of Aeronautics*, 37(2), 2024, 233-48.

[30] Bejan, A., Second law analysis in heat transfer, *Energy*, 5(8-9), 1980, 720-732.
[31] Bejan, A., Entropy generation minimization: The new thermodynamics of finite-size devices and finite-time processes, *Journal of Applied Physics*, 79(3), 1996, 1191–1218.
[32] Biswal, P., Basak, T., Entropy generation vs energy efficiency for natural convection based energy flow in enclosures and various applications: a review, *Renewable and Sustainable Energy Reviews*, 80, 2017, 1412-1457.
[33] Goh, L. H. K., Hung, Y. M., Chen, G. M., Tso, C. P., Entropy generation analysis of turbulent convection in a heat exchanger with self-rotating turbulator inserts, *International Journal of Thermal Sciences*, 160, 2021, 106652.
[34] Magherbi, M., Abbassi, H., Ben Brahim, A., Entropy generation at the onset of natural convection, *International Journal of Heat and Mass Transfer*, 46(18), 2003, 3441–3450.
[35] Ilis, G. G., Mobedi, M., Sunden, B., Effect of aspect ratio on entropy generation in a rectangular cavity with differentially heated vertical walls, *International Communications in Heat and Mass Transfer*, 35(6), 2008, 696–703.
[36] Varol, Y., Oztop, H. F., Pop, I., Entropy generation due to natural convection in non-uniformly heated porous isosceles triangular enclosures at different positions, *International Journal of Heat and Mass Transfer*, 52(5), 2009, 1193–1205.
[37] Basak, T., Kaluri, R. S., Balakrishnan, A. R., Entropy Generation During Natural Convection in a Porous Cavity: Effect of Thermal Boundary Conditions, *Numerical Heat Transfer. Part A, Applications*, 62(4), 2012, 336–364.
[38] Siavashi, M., Yousofv, R., Rezanejad, S., Nanofluid and porous fins effect on natural convection and entropy generation of flow inside a cavity, Advanced Powder Technology, *The International Journal of the Society of Powder Technology, Japan*, 29(1), 2018, 142–156.
[39] Rahaman, M. M., Bhowmick, S., Saha, S. C., Mondal, R. N., Unsteady natural convection flow of two-phase fluids within a V-shaped cavity, *AIP Conference Proceedings*, 3451(1), 2026, 070002.
[40] Gerlach, D., Tomar, G., Biswas, G., Durst, F., Comparison of volume-of-fluid methods for surface tension-dominant two-phase flows, *International Journal of Heat and Mass Transfer*, 49(3-4), 2006, 740-754.
[41] Varol, Y., Oztop, H. F., Koca, A., Entropy generation due to conjugate natural convection in enclosures bounded by vertical solid walls with different thicknesses, *International Communications in Heat and Mass Transfer*, 35(5), 2008, 648–656.
[42] Varol, Y., Oztop, H. F., Koca, A., Entropy production due to free convection in partially heated isosceles triangular enclosures, *Applied Thermal Engineering*, 28(11), 2008, 1502–1513.
[43] Rahaman, M. M., Bhowmick, S., Saha, G., Xu F., Saha, S. C., Transition to chaotic flow, bifurcation, and entropy generation analysis inside a stratified trapezoidal enclosure for varying aspect ratio, *Chinese Journal of Physics*, 91, 2024, 867-882.
[44] Yan, X., Chen, G., An approximation approach for the simulation of vapor-liquid phase change by the volume-of-fluid method, *International Journal of Multiphase Flow*, 136, 2021, 103359.
[45] Patankar, S.V., Spalding, D.B., A calculation procedure for heat, mass and momentum transfer in three-dimensional parabolic flows, *International Journal of Heat and Mass Transfer*, 15(10), 1972, 1787-1806.
[46] Leonard, B.P., A stable and accurate convective modelling procedure based on quadratic upstream interpolation, *Computer Methods in Applied Mechanics and Engineering*, 19(1), 1979, 59-98.
[47] Iyican, L., Witte, L.C., Bayazitoglu, Y., An experimental study of natural convection in trapezoidal enclosures, *Journal of Heat Transfer*, 102(3), 1980, 648–653.
[48] Baliga, B. R., Pham, T. T., Patankar, S. V., Solution of some Two-dimensional Incompressible Fluid Flow and Heat Transfer Problems, Using a Control Volume Finite-Element Method, *Numerical Heat Transfer*, 6, 1983, 263–282.
[49] Lasfer, K., Bouzaiane, M., Lili, T., Numerical study of laminar natural convection in a side-heated trapezoidal cavity at various inclined heated sidewalls, *Heat Transfer Engineering*, 31, 2010, 362–373.
[50] Basak, T., Roy, S., Pop, I., Heat flow analysis for natural convection within trapezoidal enclosures based on heatline concept, *International Journal of Heat and Mass Transfer*, 52(11-12), 2009, 2471-2483.
[51] Moukalled, F., Darwish, M., Natural convection in a trapezoidal enclosure heated from the side with a baffle mounted on its upper inclined surface, *Heat Transfer Engineering*, 25(8), 2004, 80-93.
[52] Wolf, A., Swift, J. B., Swinney, H. L., Vastano, J. A., Determining Lyapunov exponents from a time series, *Physica D: Nonlinear Phenomena*, 16(3), 1985, 285-317.

ORCID iD

Md. Mahafujur Rahaman https://orcid.org/0000-0002-7101-3314
Sidhartha Bhowmick https://orcid.org/0000-0002-9079-5809
Goutam Saha https://orcid.org/0000-0001-6467-298x
Suvash C. Saha https://orcid.org/0000-0002-9962-8919

How to cite this article: Rahaman M.M., et al. Numerical Investigation of Two-Phase Flow Transition and Heat Transfer in a V-Shaped Cavity with Stratified Fluids, *J. Appl. Comput. Mech.*, xx(x), 2026, 1–15. https://doi.org/10.22055/jacm.2026.49109.5741